AIAA Paper 95-1670

EFFECT OF ARTIFICIAL DIFFUSION SCHEMES ON MULTIGRID CONVERGENCE

Seokkwan Yoon *, Antony Jameson †, and Dochan Kwak ‡
NASA Ames Research Center
Moffett Field, California 94035

Abstract

The effect of artificial diffusion schemes on the convergence of an implicit method is investigated. A multigrid code using a symmetric limited positive scheme in conjunction with a lower-upper symmetric-Gauss-Seidel method is developed for viscous compressible flows. The present numerical method is shown to be an effective multigrid driver in three-dimensions. Despite its reasonably fast convergence, the present code requires low computational work per iteration. The symmetric limited positive scheme improves the convergence characteristics of the implicit method on a high cell aspect ratio grid. The numerical results compare well with available experimental data.

I. Introduction

It has been known that non-oscillatory finite volume schemes can be constructed through the introduction of artificial diffusion which produces an upwind bias. One approach to the construction of high resolution schemes which combine monotonicity and high order accuracy is to blend low and high order diffusive terms as in the Jameson-Schmidt-Turkel (JST) scheme.[1] Another approach to the construction of high order schemes is to add limited anti-diffusive terms to a low order scheme. An example is a family of symmetric limited positive (SLIP) schemes.[2,3]

Multigrid methods have been useful for accelerating the convergence of iterative schemes. Jameson's method[4] in conjunction with the explicit Runge-Kutta scheme has been particularly efficient for the Euler equations. The explicit multigrid method has demonstrated impressive convergence rates by taking large time steps and propagating waves fast on coarse meshes. It does not seem to be profitable to consider an unfactored implicit scheme for a multigrid driver since the implicit scheme can take large time steps which are limited by the physics rather than the grid. However, the multigrid method can improve the convergence rates of factored implicit schemes.[5,6]

Although conventional implicit methods often achieve fast convergence rates, they suffer from greater computer time per iteration than explicit methods. Yoon and Jameson[7] has introduced an implicit algorithm based on a lower-upper(LU) factorization, symmetric Gauss-Seidel(SGS) relaxation, and Newton-like iteration. The scheme has been used successfully in computing chemically reacting flows due in part to the algorithm's property which reduces the size of the left hand side matrix for nonequilibrium flows with finite rate chemistry. It has been demonstrated by Yoon and Kwak[8-10] that the LU-SGS scheme requires less CPU time per iteration than most existing time-marching methods on Cray supercomputers. However, it has been observed that the convergence rate of the multigrid LU-SGS method in conjunction with the JST scheme slows down significantly after the residual drops about four orders of magnitude on highly clustered grids. One of the objectives of the present work is to study the effect of artificial diffusion schemes on the terminal convergence characteristics of the LU-SGS method.

II. Governing Equations

Let t be time; ρ, p, and T the density, pressure, and temperature; u, v, and w the velocity components in Cartesian coordinates (x, y, z); $\widehat{Q}$ the vector of conserved variables; $\widehat{E}$, $\widehat{F}$, and $\widehat{G}$ the convective flux vectors; and $\widehat{E}_v$, $\widehat{F}_v$, and $\widehat{G}_v$ the flux vectors

* Research Scientist, Advanced Computational Methods Branch
† Visiting Scientist, Professor, Princeton University
‡ Chief, Advanced Computational Methods Branch

for the viscous terms. Then the three-dimensional Navier-Stokes equations in generalized curvilinear coordinates (ξ, η, ζ) can be written as

$$\partial_t \hat{Q} + \partial_\xi(\hat{E} - \hat{E}_v) + \partial_\eta(\hat{F} - \hat{F}_v) + \partial_\zeta(\hat{G} - \hat{G}_v) = 0 \quad (1)$$

The equation of state is needed to complete the set of equations for compressible flow.

$$p = (\gamma - 1)[e - \frac{1}{2}\rho(u^2 + v^2 + w^2)] \quad (2)$$

where γ is the ratio of specific heats.

III. Artificial Diffusion

A semidiscrete finite volume method is used to ensure the final converged solution be independent of the time step and to avoid metric singularity problems. The finite volume method is augmented by artificial diffusion terms in order to suppress the tendency for odd and even point decoupling. Artificial diffusion terms are often called filters since they work like low pass filters which damp out high frequency modes.

Consider the one-dimensional conservation law

$$\frac{\partial v}{\partial t} + \frac{\partial}{\partial x} f(v) = 0 \quad (3)$$

for a scalar dependent variable v. If Eq. (3) is represented by a three-point scheme

$$\frac{dv_j}{dt} = c^+_{j+\frac{1}{2}}(v_{j+1} - v_j) + c^-_{j-\frac{1}{2}}(v_{j-1} - v_j), \quad (4)$$

the scheme is local extremum diminishing(LED) if

$$c^+_{j+\frac{1}{2}} \geq 0, \; c^-_{j-\frac{1}{2}} \geq 0. \quad (5)$$

Eq. (3) can be approximated by a conservative semidiscrete scheme

$$\Delta x \frac{dv_j}{dt} + (h_{j+\frac{1}{2}} - h_{j-\frac{1}{2}}) = 0 \quad (6)$$

where $h_{j+\frac{1}{2}}$ is an estimate of the numerical flux between cells j and $j+1$. Since the arithmetic average of the flux leads to a scheme that does not satisfy the positivity conditions, a diffusive flux d is added to the convective flux in a conservative manner.

$$h_{j+\frac{1}{2}} = \frac{1}{2}(f_{j+1} + f_j) - d_{j+\frac{1}{2}} \quad (7)$$

where

$$d_{j+\frac{1}{2}} = \alpha_{j+\frac{1}{2}}(v_{j+1} - v_j) \quad (8)$$

The LED condition is satisfied if

$$\alpha_{j+\frac{1}{2}} \geq \frac{1}{2} \mid a_{j+\frac{1}{2}} \mid \quad (9)$$

where the wave speed $a(v) = \frac{\partial f}{\partial v}$. The least diffusive first order scheme which satisfies the LED condition can be obtained by taking

$$\alpha_{j+\frac{1}{2}} = \frac{1}{2} \mid a_{j+\frac{1}{2}} \mid \quad (10)$$

This is known as the first order upwind scheme.

Higher order non-oscillatory schemes can be derived by introducing anti-diffusive terms in a controlled manner. An early attempt is the JST scheme.

$$\begin{aligned} d_{j+\frac{1}{2}} =& \epsilon^{(2)}_{j+\frac{1}{2}} \Delta v_{j+\frac{1}{2}} \\ & - \epsilon^{(4)}_{i+\frac{1}{2}}(\Delta v_{j+\frac{3}{2}} - 2\Delta v_{j+\frac{1}{2}} + \Delta v_{j-\frac{1}{2}}) \end{aligned} \quad (11)$$

For a system of multidimensional equations the coefficients of the dissipative terms are the directionally

scaled spectral radii of the Jacobian matrices for inviscid flux vectors. Third order terms formed from fourth differences provide the background damping. First order terms are added by second differences near shock waves under the control of a sensor, $\tilde{\nu}$.

$$\tilde{\nu}_{i+\frac{1}{2}} = max(\nu_{i+1}, \nu_i) \tag{12}$$

where

$$\nu_i = max(\nu_i^p, \nu_i^T) \tag{13}$$

$$\nu_i^p = \mid p_{i+1} - 2p_i + p_{i-1} \mid / (p_{i+1} + 2p_i + p_{i-1}) \tag{14a}$$

$$\nu_i^T = \mid T_{i+1} - 2T_i + T_{i-1} \mid / (T_{i+1} + 2T_i + T_{i-1}) \tag{14b}$$

Here p and T are the pressure and the temperature. The low order dissipative coefficient is proportional to the sensor $\tilde{\nu}$ as

$$\epsilon^{(2)}_{i+\frac{1}{2}} = \kappa^{(2)} r(\widehat{A})_{i+\frac{1}{2}} \tilde{\nu}_{i+\frac{1}{2}} \tag{15}$$

where $r(\widehat{A})$ denotes the spectral radius of the Jacobian matrix $\widehat{A}$. The high order dissipative coefficient is controlled by the sensor.

$$\epsilon^{(4)}_{i+\frac{1}{2}} = max(0, \kappa^{(4)} r(\widehat{A})_{i+\frac{1}{2}} - \epsilon^{(2)}_{i+\frac{1}{2}}) \tag{16}$$

Here $\kappa^{(2)}$ and $\kappa^{(4)}$ are constants.

Since the constant total enthalpy is not preserved in general except for the Euler equations, the dissipation for the energy equation is based on the total energy rather than the total enthalpy. It has been shown that the convergence rate on high cell aspect ratio meshes can be enhanced by multiplying a scaling factor based on local cell aspect ratio to the dissipative coefficients. However, this technique has not been used here because the aspect ratio based scaling factor seems to compromise the accuracy of the solution.[11]

An alternative route is to introduce flux limiters. A simple way to introduce limiters is to use flux limited dissipation. Let $L(u, v)$ be a limited average of u and v with the following properties:

P1. $L(u, v) = L(v, u)$

P2. $L(\alpha u, \alpha v) = \alpha L(u, v)$

P3. $L(u, u) = u$

P4. $L(u, v) = 0$ if u and v have opposite signs.

Properties (P1-P3) are natural properties of an average. Property P4 is needed for the construction of an LED scheme.

The diffusive flux for a scalar conservation law is defined as

$$d_{j+\frac{1}{2}} = \alpha_{j+\frac{1}{2}} \{\Delta v_{j+\frac{1}{2}} - L(\Delta v_{j+\frac{3}{2}}, \Delta v_{j-\frac{1}{2}})\}. \tag{17}$$

Also define

$$r^{\pm} = \frac{\Delta v_{j\pm\frac{3}{2}}}{\Delta v_{j\mp\frac{1}{2}}} \tag{18}$$

and

$$\phi(r) = L(1, r) = L(r, 1). \tag{19}$$

Then the scheme satisfies the LED condition if $\alpha_{j+\frac{1}{2}} \geq \frac{1}{2} \mid a_{j+\frac{1}{2}} \mid$ for all j, and $\phi(r) \geq 0$, which is assured by property P4 on L. At the same time it follows from property P3 that the first order diffusive flux is canceled when Δv is smoothly varying and of constant sign. Schemes constructed by this formulation are referred to as the symmetric limited positive (SLIP) schemes[2].

A variety of limiters may be defined which meet the requirements of properties P1-P4. Define

$$S(u, v) = \frac{1}{2}\{sign(u) + sign(v)\} \tag{20}$$

so that

$$S(u, v) = \begin{bmatrix} 1 \; if \; u > 0 \; and \; v > 0 \\ 0 \; if \; u \; and \; v \; have \; opposite \; signs \\ -1 \; if \; u < 0 \; and \; v < 0 \end{bmatrix}$$

Three limiters which are appropriate are the following well-known schemes.

1. Minmod:

$$L(u,v) = S(u,v)min(\mid u \mid, \mid v \mid) \tag{21}$$

2. Van Leer:

$$L(u,v) = S(u,v)\frac{2 \mid u \mid\mid v \mid}{\mid u \mid + \mid v \mid} \tag{22}$$

3. Superbee:

$$L(u,v) = S(u,v)max\{min(2 \mid u \mid, \mid v \mid),$$

$$min(\mid u \mid, 2 \mid v \mid)\} \tag{23}$$

These limiters are unnecessarily stringent. Superbee, for example, could be relaxed to α-bee.

4. α-bee:

$$L(u,v) = S(u,v)max\{min(\alpha \mid u \mid, \mid v \mid),$$

$$min(\mid u \mid, \alpha \mid v \mid)\} \tag{24}$$

This limiter reduces to minmod when α=1, and less stringent than Superbee when $\alpha > 2$. Superbee differs from the other limiters in that it introduces a larger amount of antidiffusion than that needed to cancel the diffusion. Thus it tends to produce artificial compression of discontinuities. A generalized limiter contains the first two limiters.

5. Jameson:

$$L(u,v) = \frac{1}{2}D(u,v)(u+v) \tag{25}$$

where $D(u,v)$ is a factor which should deflate the arithmetic average, and becomes zero if u and v have opposite signs.

$$D(u,v) = 1 - \left[\frac{u-v}{\mid u \mid + \mid v \mid}\right]^k \tag{26}$$

where k is a positive integer. Then $D(u,v) = 0$ if u and v have opposite signs. Also if $k = 1$, $L(u,v)$ reduces to minmod, while if $k = 2$, $L(u,v)$ is equivalent to Van Leer's limiter. By increasing k one can generate a sequence of limited averages which approach a limit set by the arithmetic mean truncated to zero when u and v have opposite signs.

IV. Multigrid Method

In the present multigrid method, part of the task of tracking the evolution of the solution is transferred through a sequence of successively coarser meshes. The use of larger control volumes on the coarser meshes tracks the large scale evolution, with the consequence that global equilibrium can be more rapidly attained. This evolution on the coarse grid is driven by the solution of the fine grid equations. The solution vector on a coarse grid is initialized as

$$Q_{2h}^{(0)} = \Sigma S_h Q_h / S_{2h} \tag{27}$$

where the subscripts denote values of the mesh spacing parameter h, S is the cell volume, and the sum is over the eight cells of the fine grid which compose each cell of the coarse grid. After updating the fine grid solution, the values of the conserved variables are transferred to the coarse grid using Eq. (27). The pressure is calculated on the coarse grid using the transferred variables. Then a forcing function is defined as

$$P_{2h} = \Sigma R_h(Q_h) - R_{2h}(Q_{2h}^{(0)}) \tag{28}$$

where R is the residual.

The residual on the coarse grid is given by

$$R_{2h}^{*} = R_{2h}(Q_{2h}) + P_{2h} \tag{29}$$

For the next coarser grid, the residual is calculated as

$$R^*_{4h} = R_{4h}(Q_{4h}) + P_{4h} \tag{30}$$

where

$$P_{4h} = \Sigma R^*_{2h} - R_{4h}(Q^{(0)}_{4h}) \tag{31}$$

The process is repeated on successively coarser grids. Multiple iterations can be done on each coarse grid. Artificial diffusion terms for the coarse grids are formed from second differences with constant coefficients. Finally, the correction calculated on each grid is interpolated back to the next finer grid. Let $\tilde{Q}_{2h}$ be the final value of Q_{2h} resulting from both the correction calculated on grid $2h$ and the correction transferred from the grid $4h$. Then

$$\tilde{Q}_h = Q_h + I^h_{2h}(\tilde{Q}_{2h} - Q^{(0)}_{2h}) \tag{32}$$

where Q_h is the solution on grid h before the transfer to the grid $2h$, and I is a trilinear interpolation operator.

V. LU-SGS Implicit Scheme

The governing equations are integrated in time for both steady and unsteady flow calculations. For a steady-state solution, the use of a large time step leads to fast convergence. For a time-accurate solution, it is desirable that the time step is determined by the physics rather than the numerics. An unfactored implicit scheme can be obtained from a nonlinear implicit scheme by linearizing the flux vectors about the previous time step and dropping terms of the second and higher order.

$$[I + \alpha\Delta t(D_\xi \hat{A} + D_\eta \hat{B} + D_\zeta \hat{C})]\delta\hat{Q} = -\Delta t\hat{R} \tag{33}$$

where $\hat{R}$ is the residual

$$\hat{R} = D_\xi(\hat{E} - \hat{E}_v) + D_\eta(\hat{F} - \hat{F}_v) + D_\zeta(\hat{G} - \hat{G}_v) \tag{34}$$

and I is the identity matrix. $\delta\hat{Q}$ is the correction $\hat{Q}^{n+1}$ - $\hat{Q}^n$, where n denotes the time level. D_ξ, D_η, and D_ζ are difference operators that approximate ∂_ξ, ∂_η, and ∂_ζ. $\hat{A}$, $\hat{B}$, and $\hat{C}$ are the Jacobian matrices of the convective flux vectors.

$$\hat{A} = \frac{\partial\hat{E}}{\partial\hat{Q}}, \quad \hat{B} = \frac{\partial\hat{F}}{\partial\hat{Q}}, \quad \hat{C} = \frac{\partial\hat{G}}{\partial\hat{Q}} \tag{35}$$

For $\alpha = \frac{1}{2}$, the scheme is second order accurate in time. For other values of α, the time accuracy drops to first order. Although the direct inversion method seems to be competitive with approximate factorization methods in the overall computing time in two-dimensions, direct inversion of a large block banded matrix of the unfactored scheme Eq. (33) appears to be impractical in three-dimensions because of the rapid increase of the number of operations as the number of mesh points increases and because of the large memory requirement.

To alleviate this difficulty, Yoon and Jameson[7] derived an efficient implicit algorithm by combining the advantages of LU factorization, SGS relaxation, and Newton iteration. The LU-SGS scheme can be written as

$$LD^{-1}U\delta\hat{Q} = -\Delta t\hat{R} \tag{36}$$

where

$$\begin{aligned} L &= I + \alpha\Delta t(D^-_\xi \hat{A}^+ + D^-_\eta \hat{B}^+ + D^-_\zeta \hat{C}^+ - \hat{A}^- - \hat{B}^- - \hat{C}^-) \\ D &= I + \alpha\Delta t(\hat{A}^+ - \hat{A}^- + \hat{B}^+ - \hat{B}^- + \hat{C}^+ - \hat{C}^-) \\ U &= I + \alpha\Delta t(D^+_\xi \hat{A}^- + D^+_\eta \hat{B}^- + D^+_\zeta \hat{C}^- + \hat{A}^+ + \hat{B}^+ + \hat{C}^+) \end{aligned} \tag{37}$$

where D^-_ξ, D^-_η, and D^-_ζ are backward difference operators, while D^+_ξ, D^+_η, and D^+_ζ are forward difference operators.

In the framework of the LU-SGS algorithm, a variety of schemes can be developed by different choices

of numerical dissipation models and Jacobian matrices of the flux vectors. The matrix should be diagonally dominant to ensure convergence to a steady state. Jacobian matrices leading to diagonal dominance are constructed so that " + " matrices have nonnegative eigenvalues while "−" matrices have nonpositive eigenvalues. For example,

$$\begin{aligned} \hat{A}^{\pm} &= \hat{T}_{\xi}\Lambda_{\xi}^{\pm}\hat{T}_{\xi}^{-1} \\ \hat{B}^{\pm} &= \hat{T}_{\eta}\Lambda_{\eta}^{\pm}\hat{T}_{\eta}^{-1} \\ \hat{C}^{\pm} &= \hat{T}_{\zeta}\Lambda_{\zeta}^{\pm}\hat{T}_{\zeta}^{-1} \end{aligned} \tag{38}$$

where typically $\hat{T}_{\xi}$ and $\hat{T}_{\xi}^{-1}$ are similarity transformation matrices of the eigenvectors of $\hat{A}$. Another possibility is to construct Jacobian matrices of the flux vectors approximately to yield diagonal dominance.

$$\begin{aligned} \hat{A}^{\pm} &= \frac{1}{2}[\hat{A} \pm \sigma(\hat{A})I] \\ \hat{B}^{\pm} &= \frac{1}{2}[\hat{B} \pm \sigma(\hat{B})I] \\ \hat{C}^{\pm} &= \frac{1}{2}[\hat{C} \pm \sigma(\hat{C})I] \end{aligned} \tag{39}$$

where

$$\sigma(\hat{A}) = \tilde{\kappa}\ max[|\ \lambda(\hat{A})\ |] \tag{40}$$

Here $\lambda(\hat{A})$ represent eigenvalues of the Jacobian matrix $\hat{A}$ and $\tilde{\kappa}$ is a constant that is greater than or equal to 1. A typical value of $\tilde{\kappa}$ is 1. However, stability and convergence can be controlled by adjusting $\tilde{\kappa}$ as the flowfield develops. The diagonal matrix of eigenvalues is

$$\hat{\Lambda}(\hat{A}) = \begin{bmatrix} U & 0 & 0 & 0 & 0 \\ 0 & U & 0 & 0 & 0 \\ 0 & 0 & U & 0 & 0 \\ 0 & 0 & 0 & U+C_{\xi} & 0 \\ 0 & 0 & 0 & 0 & U-C_{\xi} \end{bmatrix} \tag{41}$$

and

$$C_{\xi} = c\sqrt{\xi_x^2 + \xi_y^2 + \xi_z^2} \tag{42}$$

where c is the speed of sound:

$$c = \sqrt{\frac{\gamma p}{\rho}} \tag{43}$$

Eq. (36) can be inverted in three steps:

$$\begin{aligned} \delta\hat{Q}^{*} &= -\Delta t L^{-1}\hat{R} \\ \delta\hat{Q}^{**} &= D\delta\hat{Q}^{*} \\ \delta\hat{Q} &= U^{-1}\delta\hat{Q}^{**} \end{aligned} \tag{44}$$

It is interesting to note that the need for block inversions along the diagonals can be eliminated if we use the approximate Jacobian matrices of Eq. (39). Setting $\alpha = 1$ and $\Delta t = \infty$ yields a Newton-like iteration. Although a quadratic convergence of the Newton method cannot be achieved because of the approximate factorization, a linear convergence can be demonstrated. That is why the term Newton-like instead of Newton is used to distinguish the differences. The use of Newton-like iteration offers a practical advantage that one does not have to waste time to find an optimal Courant number or time step. If two-point one-sided differences are used, Eq. (37) reduces to

$$\begin{aligned} L &= \sigma I - \hat{A}^{+}_{i-1,j,k} - \hat{B}^{+}_{i,j-1,k} - \hat{C}^{+}_{i,j,k-1} \\ D &= \sigma I \\ U &= \sigma I + \hat{A}^{-}_{i+1,j,k} + \hat{B}^{-}_{i,j+1,k} + \hat{C}^{-}_{i,j,k+1} \end{aligned} \tag{45}$$

where

$$\sigma = \sigma(\hat{A}) + \tilde{\sigma}(\hat{B}) + \tilde{\sigma}(\hat{C}) \tag{46}$$

In the inversion process, $\hat{A}^{+}_{i-1,j,k}$ is multiplied by $\delta\hat{Q}^{*}_{i-1,j,k}$, for example. The algorithm permits scalar diagonal inversions since σ is scalar.

VI. Vectorization

The algorithm is completely vectorizable on $i+j+k = constant$ diagonal planes of sweep. This is achieved by reordering the arrays.

$$\hat{Q}(ipoint, iplane) = \hat{Q}(i,j,k) \tag{47}$$

where *iplane* is the serial number of the diagonal plane, and *ipoint* is the address on that plane. Let

$imax$, $jmax$, and $kmax$ be maximum number of grid points at each coordinate direction. Then the number of diagonal planes for cell-centers is given by

$$nplane = imax + jmax + kmax - 5 \qquad (48)$$

with the maximum vector length of

$$npoint = (jmax - 1) * (kmax - 1) \qquad (49)$$

when

$$imax = max(imax, jmax, kmax) \qquad (50)$$

VII. Results

In order to investigate the effect of artificial diffusion schemes on the convergence, transonic flow calculations have been carried out for an ONERA M6 wing. A 193 x 49 x 33 C-O grid (312,081 points) with high cell aspect ratios is used. Here 49 grid points are used in the normal direction. The distance of the first normal grid point from the wing surface is 1.3 x 10^{-5} times the chord length. Fig. 1 shows the distribution of geometric cell aspect ratios of the first normal mesh cells at the body from the leading edge to the downstream boundary. The cell aspect ratios on the wing reach as high as 1,000.

Test cases include both attached and separated flow conditions. The freestream conditions for the attached flow are are at a Mach number of 0.8395, and a 3.06° angle of attack. Since this is an unseparated flow case, the solution of the Euler equations is first considered. Fig. 2 shows single grid convergence histories of the root-mean-squared residuals which correspond to the density corrections. The residuals are normalized by their initial values. Convergence histories of two different artificial diffusion schemes are compared. The dashed line indicates the JST scheme while the solid line indicates the SLIP scheme. Aspect ratio based scaling factors have not been used for the JST scheme. According to the authors' experience, the convergence rates of the LU-SGS scheme on C-O grids are about twice slower than those on C-H grids. Nevertheless, residuals of both artificial diffusion schemes drop four and half orders of magnitude at the approximately same rates. However, the JST scheme's residual stops converging at five orders of magnitude while the SLIP scheme's residual drops nearly seven orders of magnitude. Single grid lift convergence histories in Fig. 3 indicate that the JST scheme fails to reach to a steady state in this case.

Fig. 4 shows multigrid convergence histories using a four-level V-cycle with two iterations on each coarse grid. The convergence rate of the JST scheme slows down significantly after the residual drops about four orders of magnitude. The residual of the SLIP scheme drops nearly seven orders of magnitude. Multigrid lift convergence histories in Fig. 5 show that the SLIP scheme reaches a steady state earlier than the JST scheme.

Convergence histories of the SLIP scheme on both single and multiple grids are compared in Figs. 6 and 7. The dashed line indicates the single grid while the solid line indicates the multigrid. Fig. 6 shows that four orders of residual drop requires 1,680 and 220 iterations, while six orders of residual drop requires 7,860 and 1,180 iterations for single and multigrid respectively. The convergence based on residuals has been accelerated by a factor of 7 in terms of iterations by the use of the multigrid method. Fig. 7 shows that the lift coefficients reach within the 0.5% of the final value in 5,960 and 260 iterations for single and multigrid respectively. The convergence based on lift coefficients has been accelerated by a factor of 23 in terms of iterations by the use of the multigrid method. However, a multigrid cycle requires more time per iteration than a single grid cycle not only because of additional operations for transfer and interpolation but because of the short vector lengths on the coarse grids. The overhead for the multigrid cycle in this case is approximately 80%. Thus the net acceleration factors are approximately 4 for residuals and 13 for lift coefficients.

Fig. 8 shows pressure coefficients at the 44% semi-span station for both experimental data[12] and the Euler solutions. The SLIP scheme appears to be able to capture nonoscillatory shocks with a sharper resolution than the JST scheme. The Navier-Stokes solutions are obtained using the SLIP scheme. The Baldwin-Lomax algebraic turbulence model is used

for closure. The Reynolds number based on the chord length at the root is 1.5 x 10^7. A comparison of pressure coefficients at the 65% semi-span station in Fig. 9 shows that the Navier-Stokes solution is closer to the experimental data than the Euler solution even for the attached flow.

The freestream conditions for the separated flow are are at a Mach number of 0.8447, and a 5.06° angle of attack. Fig. 10 shows the streaklines on the wing surface calculated using the SLIP scheme with the Balwin-Lomax turbulence model. Fig. 11 shows that the lift coefficients converge within the 0.5% of the final value in 200 iterations. Fig. 12 shows that residuals drop about four and a half orders of magnitude in 200 iterations. The present multigrid code with two coarse grid corrections requires 11 μsec per point per iteration on a Cray C90 single processor for the thin-layer Navier-Stokes equations using the Baldwin-Lomax turbulence model and the SLIP scheme. Thus approximately 11 *min* of CPU time are required for convergence for this case.

Conclusions

The symmetric limited positive scheme not only produces solutions with higher accuracy than the conventional artificial diffusion model but improves the robustness and the terminal convergence of a multigrid method which uses an implicit scheme as its driver.

References

1. Jameson, A., Schmidt, W., and Turkel, E., "Numerical Solution of the Euler Equations by Finite Volume Methods Using Runge-Kutta Time Stepping Schemes," AIAA Paper 81-1259, July 1981.
2. Jameson, A., "Analysis and Design of Numerical Schemes for Gas Dynamics 1: Artificial Diffusion, Upwind Biasing, Limiters and Their Effect on Accuracy and Multigrid Convergence," Submitted to International Journal of Computational Fluid Dynamics, Aug. 1994.
3. Jameson, A., "Analysis and Design of Numerical Schemes for Gas Dynamics 2: Artificial Diffusion and Discrete Shock Structure," Submitted to International Journal of Computational Fluid Dynamics, Aug. 1994.
4. Jameson, A., "Solution of the Euler Equations for Two-Dimensional Transonic Flow by a Multigrid Method," Applied Math. and Computation, Vol. 13, Nov. 1983, pp. 327-356.
5. Jameson, A. and Yoon, S., "Multigrid Solution of the Euler Equations Using Implicit Schemes," AIAA Journal, Vol. 24, Nov. 1986, pp. 1737-1743.
6. Jameson, A. and Yoon, S., "Lower-Upper Implicit Schemes with Multiple Grids for the Euler Equations," AIAA Journal, Vol. 25, July 1987, pp. 929-935.
7. Yoon, S. and Jameson, A., "Lower-Upper Symmetric-Gauss-Seidel Method for the Euler and Navier-Stokes Equations," AIAA Journal, Vol. 26, Sep. 1988, pp. 1025-1026.
8. Yoon, S. and Kwak, D., "Three-Dimensional Incompressible Navier-Stokes Solver Using Lower-Upper Symmetric Gauss-Seidel Algorithm," AIAA Journal, Vol. 29, June 1991, pp. 874-875.
9. Yoon, S. and Kwak, D., "Implicit Navier-Stokes Solver for Three-Dimensional Compressible Flows," AIAA Journal, Vol. 30, Nov. 1992, pp. 2653-2659.
10. Yoon, S. and Kwak, D., "Multigrid Convergence of an Implicit Symmetric Relaxation Scheme," AIAA Journal, Vol. 32, May 1994, pp. 950-955.
11. Jou, W.H., Wigton, L.B., Allmaras, S.R., Spalart, P.R., and Yu, N.J., "Towards Industrial-Strength Navier-Stokes Codes," Fifth Symposium on Numerical and Physical Aspects of Aerodynamic Flows, Long Beach, California, Jan. 1992.
12. Schmitt, V. and Charpin, F., " Pressure Distributions on the ONERA M6 Wing at Transonic Mach Numbers," AGARD AR-138-B1, 1979.

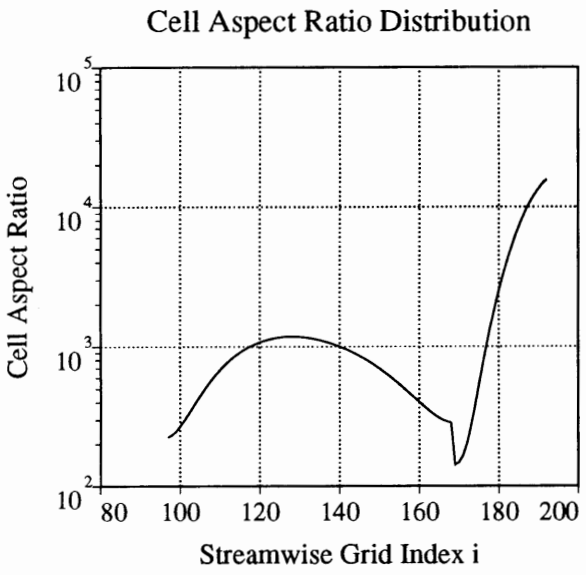

Fig. 1. Distribution of Cell Aspect Ratios

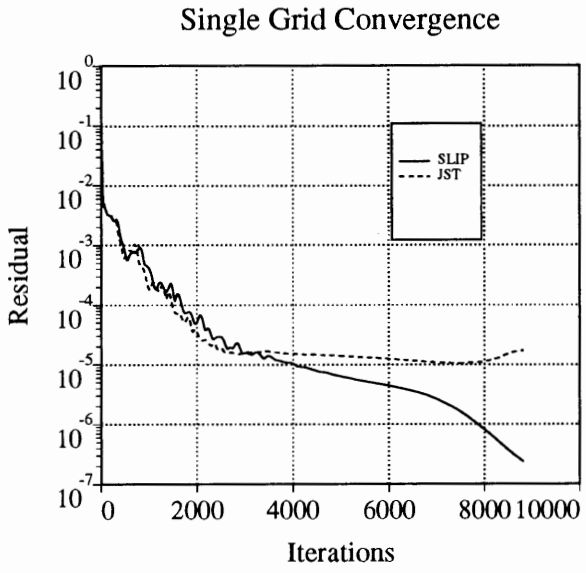

Fig. 2. Single Grid Convergence Histories

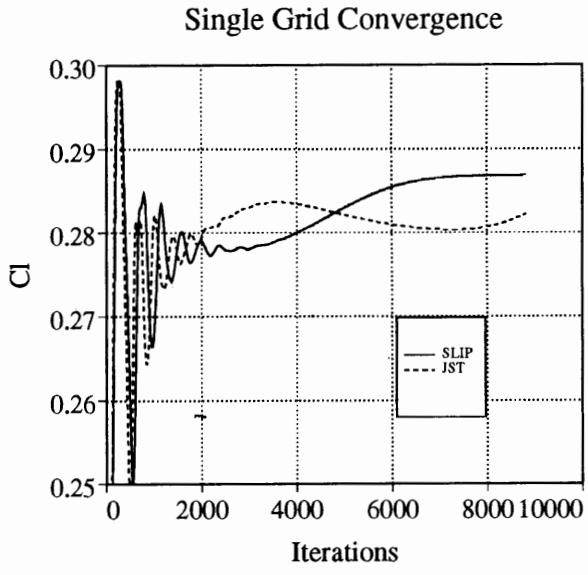

Fig. 3. Single Grid Lift Histories

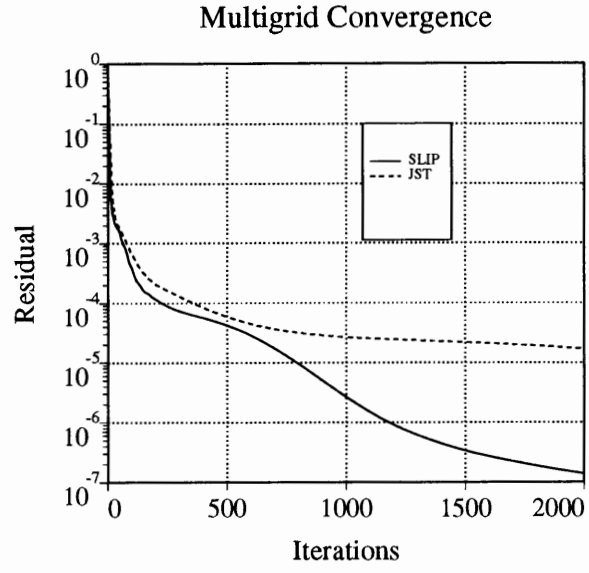

Fig. 4. Multigrid Convergence Histories

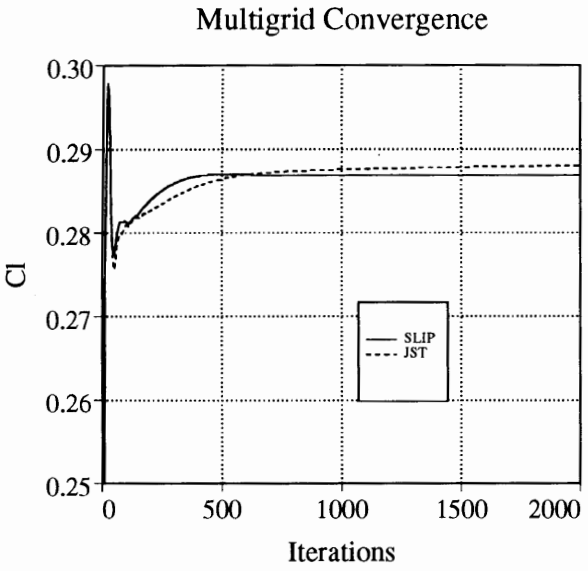

Fig. 5. Multigrid Lift Histories

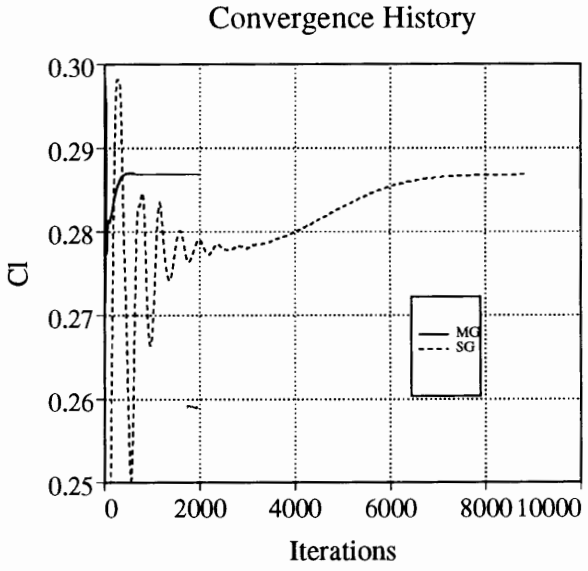

Fig. 7. SLIP Scheme Lift Histories

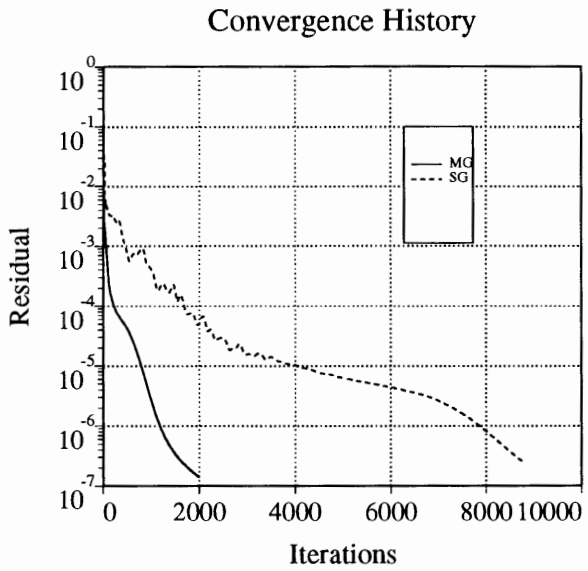

Fig. 6. SLIP Scheme Convergence Histories

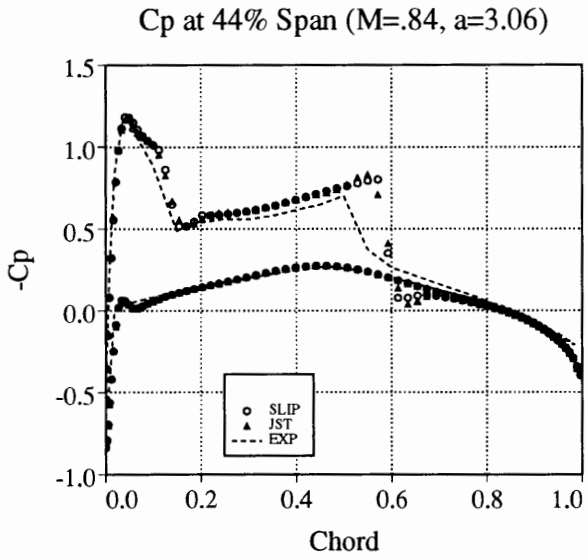

Fig. 8. C_p at 44% Span for 3.06° case

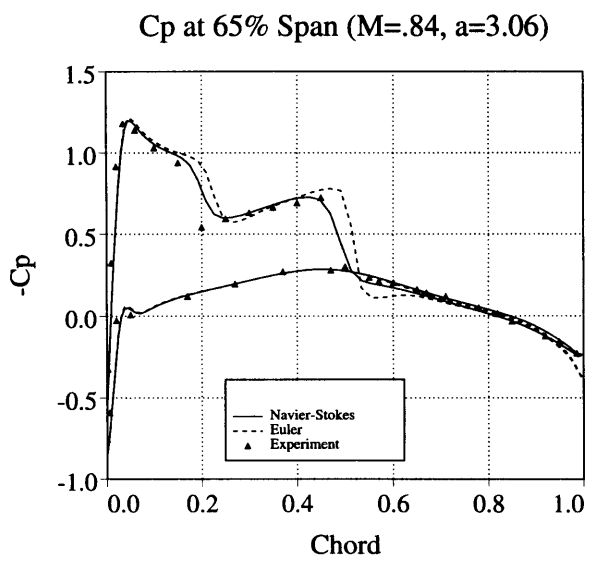

Fig. 9. C_p at 65% Span for 3.06° case

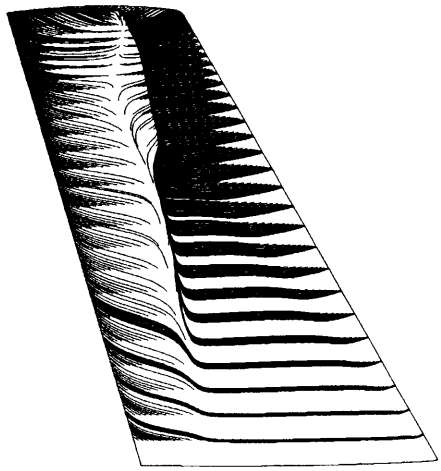

Fig.10. Surface Streaklines for 5.06° case

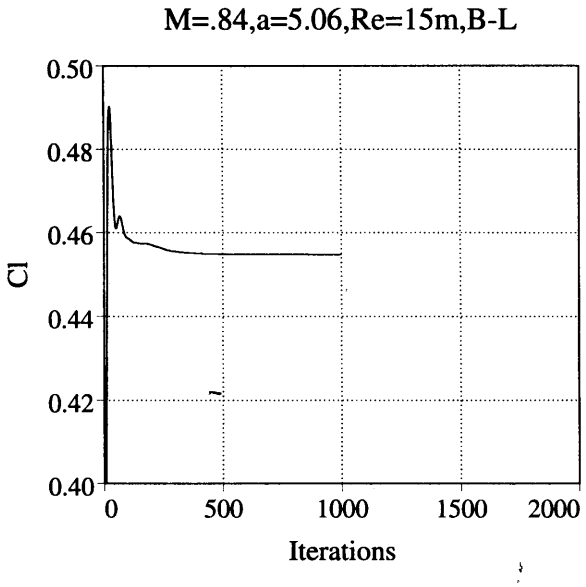

Fig.11. Lift History for 5.06° case

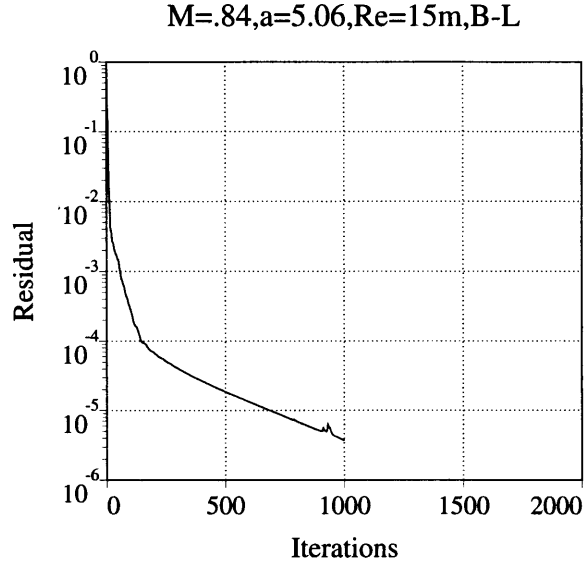

Fig.12. Residual History for 5.06° case